Journal of Electrical Engineering, Vol. 75, No. 2, 2024, pp. 124-136

sciendo

PAPERS

Performance enhancement of band-pass FIR filter-based M-class phasor estimation

Mukesh Kumar, M. Senthil Kumar

The paper presents the performance enhancement of band-pass filter-based M-class phasor estimation. The performance of the M-class phasor estimation using a band-pass FIR filter is enhanced with a magnitude correction factor for the off-nominal frequency range. The band-pass filter is implemented for the phasor estimation with various window functions Tukey, Rife Vincent class-I order-2 (RV2), Hamming, Hanning, Blackman, and Flat-top (FT) and its performance are evaluated under the steady and dynamic state tests prescribed by the standard. A rigorous performance analysis of enhanced phasor estimation using band-pass FIR filter with various window functions is presented with the accuracy indices of total vector error (TVE), frequency error (FE), and rate of change of frequency error (RFE). The result analysis reveals that the performance enhanced phasor estimation using band-pass FIR filter offers significantly less error than reported work at the low sampling rate. The design and performance analysis of the phasor estimation using the band-pass FIR filter is performed in the MATLAB platform.

Keywords: synchrophasor estimation, frequency estimation, M-class phasor measurement, phasor measurement unit, band-pass FIR filter

1 Introduction

The phasor measurement unit (PMU) measures the phasor of voltage and current signals, frequency, and rate of change of frequency (ROCOF) of voltage with reference to the synchronized time (UTC). The synchronized phasor measurement is known as synchrophasor which enables measurement, control, etc applications for a wide area of power system network, called wide area monitoring systems (WAMS). It is important to estimate the phasor accurately under dynamic conditions to have reliable monitoring, control, and protection operation performed using measured phasor [1-4]. The development of the phasor estimating technique has been subjected to a substantial amount of study as part of an effort to make the PMU more functional in WAMS. The IEEE/IEC synchrophasor standard 60255-118-1 describes the two classes of measurement i.e., *M*-class, and *P*-class [5]. It also specifies the evaluation method of phasor estimation and accuracy limit under standard test conditions.

The current industrial product of PMUs extensively uses the discrete Fourier transform (DFT) for phasor estimation as it is simple and has less computation. However, two measurement errors are rising as a result of the DFT approach [6]. First, the spectrum leakage error is produced during off-nominal frequency. Second, the static phasor model of the DFT produces the averaging effect under dynamic conditions, which adds significant errors [7].

In [8], an interpolated DFT (IpDFT) is proposed to improve the accuracy of the phasor estimation, especially under off-nominal frequency. Further, the enhanced IpDFT is proposed with the iterative process to augment the performance by compensating the effects of the self-interaction between the positive and the negative images of the spectrum [9]. Similarly, the oscillatory phenomenon of a signal is modelled using Taylor weighted least squares to estimate the phasor [10]. However, it is prone to produce errors during frequency deviation and fails to adapt anti-interference and dynamic performance capabilities simultaneously. The improved Taylor-weighted least squares method is presented for phasor estimation with the optimal coefficients and FIR filter [11].

A few methods using the Hilbert transform convolution have been developed for extracting the fundamental component of a signal under a dynamic state [12, 13]. The reference PMU signal processing model is investigated in [14-16]. Here, the filters are designed based on passband flatness and stopband rejection of the out-of-band (OOB) signal [17]. An appropriate bandpass FIR filter can be designed with the brick wall FIR filter using the windowing method as presented in [14]. It shows better performance in terms of low computation burden, fast response, high accuracy, and high rejection to both harmonic and interharmonic components. However, it uses a high sampling frequency of 6000 per sec. The reference model with the Blackman window function associated FIR filter for phasor estimation does

Department of Electrical Engineering, National Institute of Technology Patna, Bihar, 800005 India
mukeshk.phd20.ee@nitp.ac.in, msk.ee@nitp.ac.in

https://doi.org/10.2478/jee-2024-0016, Print (till 2015) ISSN 1335-3632, On-line ISSN 1339-309X

not validate with all tests of steady state and dynamic conditions [15]. Further, the reference PMU signal model is investigated in [16] and compared the various window functions i.e. Hamming, Hanning, Blackman, RV2, and FT. However, it is demonstrated that the Hamming window exhibits limit violation in frequency and ROCOF estimation. The analysis reveals failures in frequency and ROCOF when utilizing the Hamming window which is recommended in standard. The main goal of the phasor estimation techniques is to estimate the phasor corresponding to the fundamental component of a signal under steady and dynamic states. It is observed that all methods fulfil either the requirement criteria or the computational burden and are not able to satisfy both together. Therefore, it is essential to explore phasor estimation techniques further to achieve better performance at less computation.

In this context of the reported work, the paper presents the performance enhancement of the band-pass FIR filter-based phasor estimation at a low sampling rate. The performance enhancement is attained with the magnitude correction factor for the off-nominal frequency band. The performance of the phasor estimation is evaluated under all compliance tests prescribed in the IEC/IEEE standard. In addition, the performance of the enhanced band-pass FIR filter-based phasor estimation with various windows namely Hamming, Hanning, Blackman, RV2 and Flat-top is compared with the results reported in [14-16]. Further, a comprehensive analysis of the abovementioned window functions is presented. The paper is presented as follows: Section 2 describes the mathematical model of phasor estimation using the FIR filter. Section 3 discusses the designing of FIR filters using various window functions. Section 4 presents the performance analysis of the phasor estimation using an FIR filter with various window functions. Finally, section 5 gives the conclusion of the presented work.

2 Phasor representation and estimation

Let consider a sinusoidal signal $x(t)$ as

$$x(t) = x_m \cos(2\pi f_{in} t + \phi), \quad (1)$$

where x_m is the maximum magnitude of the signal, ϕ_0 is the phase angle of the signal in radians, t is the time in sec, and f_{in} is the input frequency as given in Eqn. (2).

$$f_{in} = f_0 + \Delta f \quad (2)$$

The f_0 is the nominal frequency and Δf is the frequency deviation from the nominal value. A theoretical phasor representation $X(t)$ of signal $x(t)$ is defined in (3) and presented graphically in Fig. 1.

$$X(t) = \frac{x_m}{\sqrt{2}} e^{j\phi(t)} \quad (3)$$

The $\phi(t)$ is the instantaneous phase angle of the signal given as

$$\phi(t) = (2\pi\Delta f t + \phi_0). \quad (4)$$

The input frequency of the signal (f_{in}) is the first-order derivative of $\phi(t)$

$$f_{in}(t) = f_0 + \frac{1}{2\pi}\frac{d\phi(t)}{dt}. \quad (5)$$

The ROCOF is the second-order derivative of $\phi(t)$

$$ROCOF(t) = \frac{df_{in}(t)}{dt}. \quad (6)$$

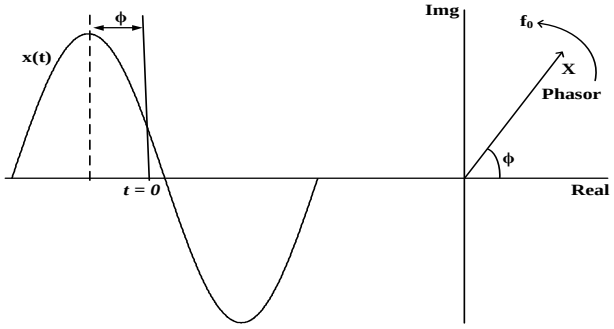

Fig. 1. Representation of phasor

The phasor estimation model of the two stages of the process is shown in Fig. 2. It consists of a band-pass FIR filter $h_c(n)$ in the first stage. In the second stage, the frequency is calculated from the phase angle obtained from the response of the band-pass FIR filter. The second stage performs the magnitude correction for the off-nominal frequency range based on the measured frequency in the second stage as the band-pass FIR filter response produces the ripples over the off-nominal frequency band. After the magnitude correction, it is combined with the phase angle measured at the first stage to represent the estimated phasor. The ROCOF is calculated from the estimated frequency.

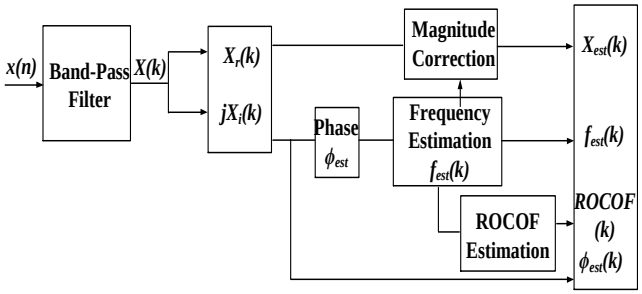

Fig. 2. Phasor estimation model

3 FIR filters for synchrophasor estimation

The frequency response of an ideal FIR filter transition sharply falls from the pass-band to the stop-band, which gives the impression of a rectangular frequency response [15]. As given in (7), the impulse response of an ideal low-pass FIR filter $h(n)$ is represented by an infinite-length sinc function as

$$h(n) = \frac{\sin(A)}{A}, \tag{7}$$

where, $A = 2\pi\frac{2F_{fr}}{fs}n;\ n = -N \ldots\ldots N$ is the filter coefficient index, f_s is the sampling frequency and F_{fr} is the reference frequency for the low-pass FIR filter.

In most cases, the impulse response of the filter is specified for a period that is limited so that it can be realized in real-time. However, high ripples in the pass band are caused by the frequency response of the fixed-length filter. The ripples in the filter's frequency response are smoothed out by multiplying the impulse response of the filter by a windowed function, as given in (8)

$$h_w(n) = h(n)W(n), \tag{8}$$

where, $W(n)$ is the window function for the length of $L = 2N + 1$, $h_w(n)$ is the impulse response of the window low-pass filter.

The impulse responses of the low-pass FIR filter and quadrature oscillator are combined in a heterodyne process at nominal frequency f_0 to obtain the band-pass FIR filter's impulse response. The band-pass filter is widened up to F_{fr} on either side of the centre f_0, hence, the band-pass includes the measurement band of interest f_{dev}

$$h_c(n) = h_w(n)e^{-\frac{i2\pi f_o n}{f_s}} \tag{9}$$

The magnitude response of the band-pass FIR filter for the input signal is obtained by convolving the discretized signal of $x(n)$ with the band-pass FIR filter function $h_c(n)$.

$$X(K) = \sum_{n=-N}^{N} x(n)h_c(k-n) \tag{10}$$

The magnitude response of the band-pass FIR filter has a ripple in the off-nominal frequency band. The enhancement of the magnitude response for off-nominal frequency is attained with the magnitude correction factor (*MCF*) obtained using the estimated frequency of the signal as given in (11).

$$MCF = \sum_{n=-N}^{N} h_w(n)e^{\frac{-2\pi f_{et} n}{f_s}} \tag{11}$$

Here, f_{et} is the estimated frequency obtained from the instantaneous phase angle $\phi_{et}(k)$ which is estimated from $X(k)$ as follows:

$$f_{et}(k) = f_o + \left(\frac{1}{2\pi}\right)\left(\frac{d\phi_{et}(k)}{dt}\right), \tag{12}$$

where $\phi_{et}(k)$ is the instantaneous phase angle of the estimated phasor as given as

$$\phi_{et}(k) = \text{atan}\left(\frac{X_i(k)}{X_r(k)}\right). \tag{13}$$

$X_r(k)$ and $X_i(k)$ are the real and imaginary terms of $X(k)$. Finally, the magnitude of the phasor is calculated with the magnitude correction factor to offer the 0 *dB* magnitude gain for the measurement frequency band of interest $f_0 + f_{dev}$. It simplifies the process of magnitude estimation over an off-nominal frequency band than the frequency tracking approaches where the quadrature oscillator adjusts to the measured frequency. Since the adaptive filtering in the frequency tracking method requires different filter coefficients according to the measured frequency, thereby it leads to high computation [18].

$$X_{etm}(k) = \frac{\sqrt{2}}{MCF} \times \sqrt{X_r^2(k) + X_i^2(k)} \tag{14}$$

MCF is the factor relating to magnitude response at estimated frequency. The correction is performed for the off-nominal frequency band to correct the ripple response caused by the first stage band-pass FIR filter. The phasor estimation is enhanced in the band-pass FIR filter using corrected magnitude $X_{etm}(k)$ and the instantaneous phase angle $\phi_{et}(k)$ as given by

$$X_{et}(k) = X_{etm}e^{j\phi_{et}t(k)}. \tag{15}$$

Further, the ROCOF is estimated as defined in (6).

This work presents a design of the performance enhanced M-class phasor estimation using a band-pass FIR filter with various window functions namely, Tukey, RV2, Hamming, Hanning, Blackman and FT window functions. The design of the band-pass FIR filter coefficient is performed in accordance with the following requirements specified in the standard for M-class phasor estimation: The magnitude gain over the passband of $f_0 \pm F_s/5$ or $\pm$ 5 Hz is 0 $\pm$ 0.043 dB. F_s represents the reporting rate. The attenuation of the signal beyond the stop-band edge frequency of $f_0 \pm F_s$ is –59.4 dB. The requirements also specify the attenuation of a 20 dB slope from $f_0 \pm F_s$ to $f_0 \pm F_s/2$. This implies extreme attenuation from $f_0 \pm F_s/2$ to $f_0 \pm F_s$ to suppress the OOB interference signal.

The presented work incorporates the F_s = 50 Hz, and the f_s = 800 Hz, thereby, the phasor estimation is

performed with the least samples of 16 samples per cycle as given in the reference model [5]. Since, it implies that the passband of the filter for 45-55 Hz, the transition band between the edge frequency of the passband and the stopband is comprised between 5 Hz to 25 Hz on both sides of the pass band, thereby the stopband of the filter lies over the range of 0 - 25 Hz and 75 Hz to maximum frequency. It should be noted that the length of the filter is determined based on the width of the transition band and it is also limited by the specification of the permissible reporting latency of $7/F_s$ for the M-class. As this work is attempted with the lowest sampling rate of 800 Hz, the maximum length of the filter is limited by 224, for F_s = 50 Hz. The following window functions are used in the band-pass FIR filter for performance analysis of phasor estimation.

a) RV2 window

It is a function of sin(x) and is also called as maximal side-lobe decay window [19].

$$W(n) = sin^{\alpha}\left(\frac{n}{N}\pi\right), \tag{16}$$

where α is normally an integer. RV2 windows are designed for minimization of the window spectrum main-lobe width (the best resolution), for a given maximum level of the side-lobe relative magnitude.

b) Hamming window

The Hamming window is an extension of the Hanning window [20]

$$W(n) = 0.54 + 0.46\cos\left(\frac{2\pi n}{N}\right). \tag{17}$$

Coefficients of the Hamming window are set to achieve minimum side-lobe levels. The Hamming window formula's coefficient is 0.54, which balances the main lobe width and side lobe level.

c) Hanning window

The Hanning window is sometimes referred to as a raised cosine window and is defined as [20]

$$W(n) = 0.5\left(1 + cos\left(\frac{2\pi n}{N}\right)\right). \tag{18}$$

Similar to the Hamming window, the Hanning window introduces a tapering effect on the signal.

d) Blackman window

The Blackman window is the one that makes use of these two-place approximations as given below.

$$W(n) = 0.42 + 0.5\cos\left(\frac{2\pi n}{N-1}\right) + 0.08\cos\left(\frac{4\pi n}{N-1}\right) \tag{19}$$

Blackman window is investigated in [20]. It contains three terms that determine the outside of the main lobe interval, putting zeros at the nominal positions of the first two sidelobes.

e) Tukey window

The Tukey window [20], is also known as the tapered cosine window. It can be regarded as a cosine lobe of width $N/2$ that is convolved with a rectangle window of width ($N/2-1$). The α is set to 2 to realize Tukey window for phasor estimation.

$$W(n) = \begin{cases} 0.5\left[1.0 + \cos\left[\pi\dfrac{n - \alpha\frac{N}{2}}{(1-\alpha)\frac{N}{2}}\right]\right], & \alpha\dfrac{N}{2} \leqslant |n| \leqslant \dfrac{N}{2} \\ 1.0, & 0 \leqslant |n| \leqslant \alpha\dfrac{N}{2} \end{cases} \tag{20}$$

f) Flat-top window

Flat-top window has a special character that differentiates them from other types of windows. This impact assessment is due to the spectral main lobe being perfectly flat or acquirable while simultaneously exhibiting fast decay of the side lobes [16]. The FT window is a cosine window, defined as

$$w(n) = \sum_{m=0}^{M} a_M[m]\cos\left(m\frac{\pi n}{N}\right), \tag{21}$$

where M = 5 is the window order of FT filter and $a_M[m]$ are the coefficients of an M-order window.

The impulse response of the window function is carefully obtained to meet the specification requirements according to the design procedure discussed [16]. The window functions RV2, Hamming, Hanning, Blackman, Tukey, and FT have been designed with a distinct reference frequency of 7.50, 7.75, 5.75, 6.65 and 5.75 (F_{fr}) Hz and length of (L) of 197, 143, 199, 197, 195 and 207 respectively, according to their characteristics. It is noted that the length of all windows is less than the maximum limit of 224. The frequency response of the FIR filter with various window functions is shown in Fig. 3.

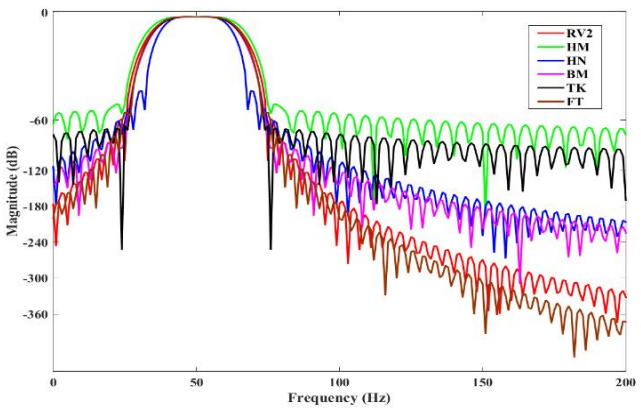

Fig. 3. FIR filter frequency response

4 Results and discussion

The performance of the enhanced phasor estimation using a band-pass FIR filter with various window functions is assessed under the standard test conditions prescribed in the IEEE/IEC standard [5] and presented in detail. The accuracy of the phasor estimating method is evaluated based on the following indices:

TVE, FE and RFE. The TVE quantifies the error between the estimated phasor value and the theoretical phasor value as given in (22).

$$TVE(n) = \sqrt{\frac{\left(X_{etr}(n) - X_{thr}(n)\right)^2 + \left(X_{eti}(n) - X_{thi}(n)\right)^2}{\left(X_{thr}(n)\right)^2 + \left(X_{thi}(n)\right)^2}} \tag{22}$$

where, $X_{etr}(n)$ and $X_{eti}(n)$ are the real and imaginary terms of the estimated phasor, $X_{thr}(n)$ and $X_{thi}(n)$ are the real and imaginary terms of the theoretical phasor values, n is the current sample instant. Similarly, the accuracy of the frequency and ROCOF measurement are evaluated using Frequency error (FE) and ROCOF error (RFE), respectively. The FE is the absolute difference between the estimated frequency and the theoretical frequency, expressed in Hz as in (23). Similarly, the RFE is the absolute difference between the estimated ROCOF and theoretical ROCOF, expressed in Hz/s as in (24).

$$FE(n) = |f_{et} - f_{th}|, \tag{23}$$

$$RFE(n) = \left|\left(\frac{df}{dt}\right)_{et} - \left(\frac{df}{dt}\right)_{th}\right|. \tag{24}$$

In addition, the step response is evaluated with delay time, response time, and overshoot.

This section presents the evaluation of the phasor, frequency, and ROCOF measurements under steady-state and dynamic-state tests prescribed in the IEC/IEEE standard [5].

4.1 Steady-state test

In the steady-state tests, the effectiveness of the phasor estimating method is assessed using steady-state sinusoidal functions that have constant values for the signal's parameters during the testing period. It consists of the following tests:

1) Frequency range test
2) Magnitude range test
3) Harmonic distortion test
4) Out-of-band interference (OOBI) test

1) Frequency range test

The frequency range test is performed with a steady-state sinusoidal signal for the range of ±5 Hz from the nominal frequency

$$x(t) = x_m \cos(2\pi f t + \phi), \tag{25}$$

where, f is $f_o + f_{dev}$, f_{dev} is the deviation of frequency from the nominal frequency by ±5 Hz, thereby the range of frequency test is carried out for 45 Hz to 55 Hz with a step of 1 Hz with the constant magnitude of 100% and constant phase angle. Under the frequency range test, the performance of the phasor estimation is evaluated using the TVE, and the results are shown in Fig. 4(a). The TVE of all window functions is almost flat for the given frequency range of ±5 Hz, except the Hamming window, which gives the maximum TVE, i.e., 0.0631 %. All other windows' TVE are much less than the Hamming. The FT and RV2 windows exhibit significantly less TVE compared to other windows. The FE is observed for all windows under the frequency range test and plotted in Fig. 4(b). It is noted that RV2 and FT windows give almost the lowest FE in the tested range. The Hanning, Blackman, and Tukey windows produce a promising maximum FE compared to other windows and fulfil the requirements criteria of 0.005 Hz maximum FE. However, the FE of Hamming window functions reaches a maximum value of 0.0045 Hz. The RFE is observed for all windows under the frequency range test and plotted in Fig. 4(c). It is evident that FT and RV2 windows give almost the lowest RFE compared to other windows. It is noted that the Tukey, RV2 and FT window consistently produces less error of TVE, FE, and RFE across the given frequency range of ±5 Hz.

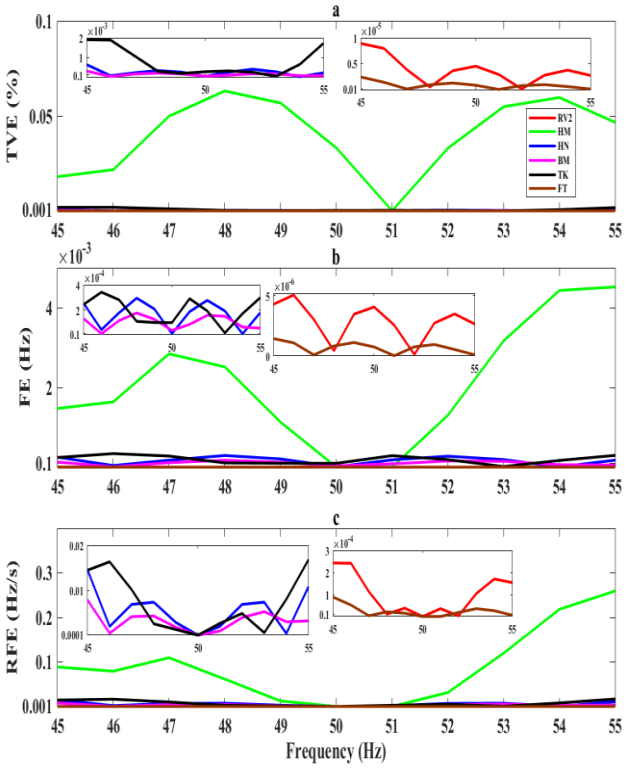

Fig. 4. (a) TVE, (b) FE, and (c) RFE under frequency range test

2) Magnitude range test

The magnitude range test is carried out using the steady-state sinusoidal signal given in (25) for the range of 10% to 120% in the step size of 10% at the nominal frequency 50 Hz and zero phase angle. As shown in Fig. 5, the TVE of all windows is consistent across the amplitude range test and well within the allowable limits. It is evident that the TVE errors are not greatly affected by the amplitude of the input signal. It is noted that the FT and RV2 windows show the lowest TVE values than the other window functions throughout the range.

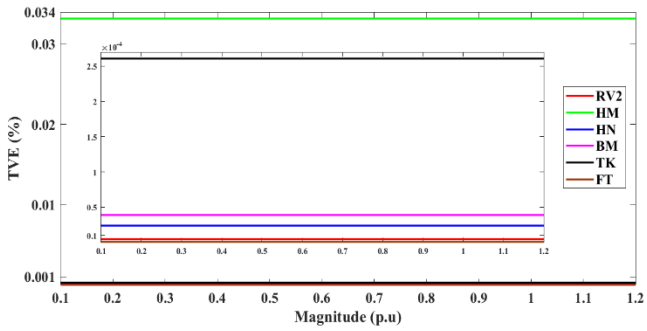

Fig. 5. TVE under magnitude range test

3) Harmonic distortion test

The test is performed with the synthesized signal of the fundamental component of 50 Hz at 100% magnitude, and 10% magnitude of the harmonic component as given in

$$x(t) = x_m \cos(2\pi f_0 t) + 0.1\, x_m \cos(2\pi f_h t), \quad (26)$$

where, f_h is the harmonic frequency which varies for the range of 2^{nd} to 50^{th} harmonic of the fundamental frequency. The performance of phasor estimation under the harmonic distortion test is shown with the TVE in Fig. 6(a). All window functions meet the criteria of 1% TVE. The performance of frequency measurement is also evaluated during the harmonic distortion test and presented in Fig. 6(b). All window functions lie below 0.025 Hz and fulfil the FE requirement criteria. The performance of ROCOF measurement is also evaluated during the harmonic distortion test and presented in Fig. 6(c). It is found that the FT and RV2 windows offer significantly less TVE, FE, and RFE values during the harmonic distortion test than the reference model (Hamming) and other window functions.

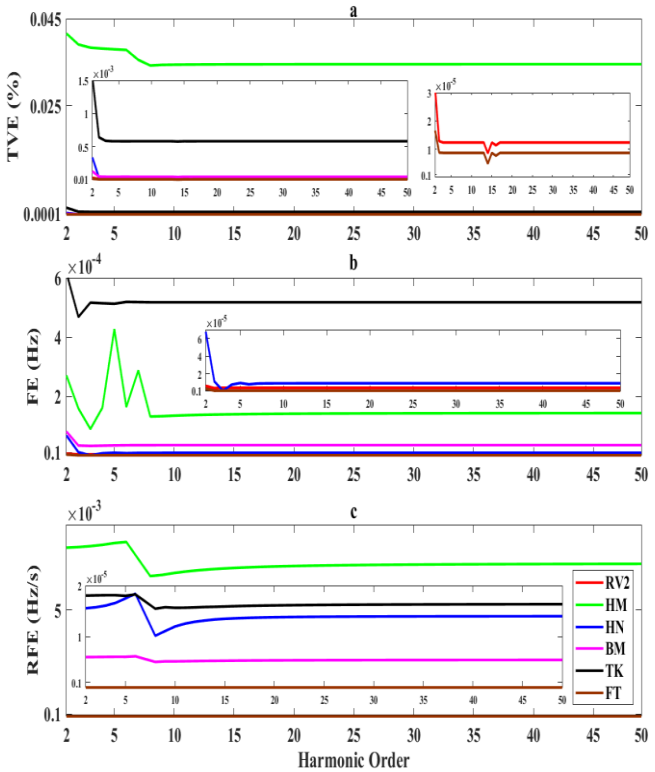

Fig. 6. (a) TVE, (b) FE, and (c) RFE under harmonic distortion test

4) OOB Interference test

The tolerance level for interharmonic pollution is evaluated using the OOB interference test. This is one of the crucial and challenging requirements for the M–class. The test signal is generated with a synthesized signal of pass band frequency signal as given in (28) at 100% magnitude and an out-of-band frequency signal at 10% magnitude given as

$$x(t) = x_m \cos(2\pi f_{in} t) + 0.1\, x_m \cos(2\pi f_{oob}\, t) \quad (27)$$

$$f_0 - 0.1\left(\frac{F_s}{2}\right) \le f_{in} \le f_0 + 0.1\left(\frac{F_s}{2}\right), \quad (28)$$

where, the f_{in} is the input frequency varies for the range of 47.5 to 52.5 Hz as given in (28). The f_{oob} is the out-of-band frequency including the frequency component beyond stop-band edge frequency (F_s/2) on either side of the passband in the range of 0 to 2^{nd} harmonic component. Hence, the out-of-band interference comprises the range of 0−25 Hz and 75−100 Hz. The TVE of all windows is below the limit of 1.3%. Interestingly, the Blackman, Hanning and Tukey windows give a lower value of TVE compared to all windows in the OOB test, as shown in Fig. 7(a). The performance of the frequency measurement is also tested under the OOB test and perceived that all windows fulfil the requirement criteria and less than the maximum FE limit of 0.01 Hz as shown in Fig. 7(b). It is also noted that Blackman gives the lowest FE than other windows which produce almost the same level of error. The effectiveness of the ROCOF measurement is also evaluated under the OOB test, and the results show that all windows of RFE as shown in Fig. 7(c). It should be highlighted that Blackman outperforms than all Windows in the ROCOF test.

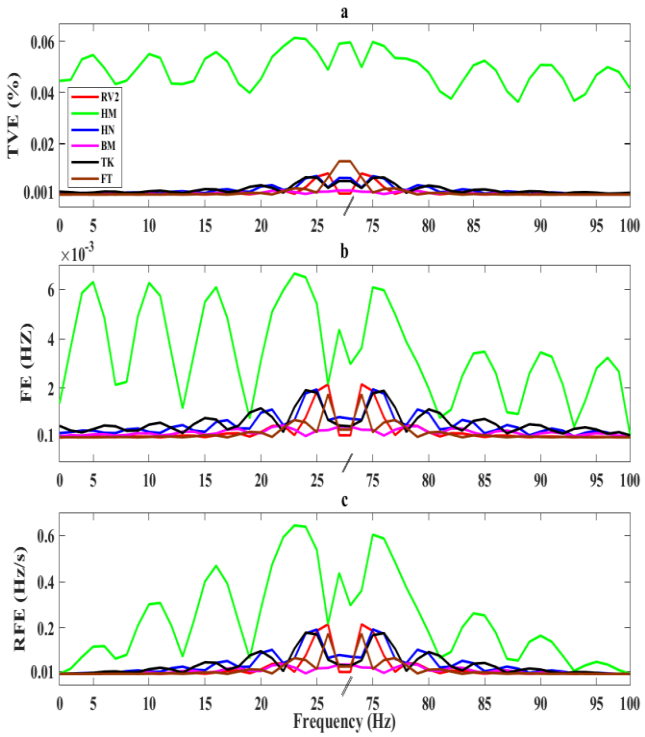

Fig. 7. (a) TVE, (b) FE, and (c) RFE under OOB interference test

4.2 Dynamic-state test

The scenario of the power system's transient condition is described by the dynamic condition. The performance of the phasor estimation under a dynamic state is investigated in the following tests:

1) Magnitude modulation test
2) Phase modulation test
3) Frequency ramp test
4) Step response test

The dynamic state is represented by a sinusoidal function that exhibits time-dependent changes in amplitude, phase, and frequency.

1) Magnitude modulation test

The signal for dynamic state magnitude modulation is modeled using (29), where the magnitude varies dynamically with the cosine function.

$$x(t) = x_m[1 + k_{mmd} \cos(\omega_{md} t)] \cos(\omega_0 t) \quad (29)$$

Here, x_m represents the maximum magnitude of signal, w_0 is the fundamental frequency in radians, w_{md} is the modulation frequency in radians, and k_{mmd} is the magnitude modulation factor. The magnitude modulation test is carried out with the k_{mmd} = 0.1, and variation of w_{md} from 0.1 to 5 Hz with a step of 0.1 Hz. The TVE of all windows under the magnitude modulation test is shown in Fig. 8(a). All windows offer much less TVE than the limits of 3%. It is noted that Tukey and FT closely trace the least of maximum TVE. The frequency measurement error under the magnitude modulation test is presented in Fig. 8(b) which shows that the FE of all windows is appreciably lower than the limit of 0.3 Hz. Further measurement error for the ROCOF under the amplitude modulation test is shown in Fig. 8(c), which demonstrates that the RFE of all windows is significantly below the limit of 14 Hz/s. The results show that the Tukey and FT windows perform exceptionally well in terms of TVE, FE, and RFE in the magnitude modulation test.

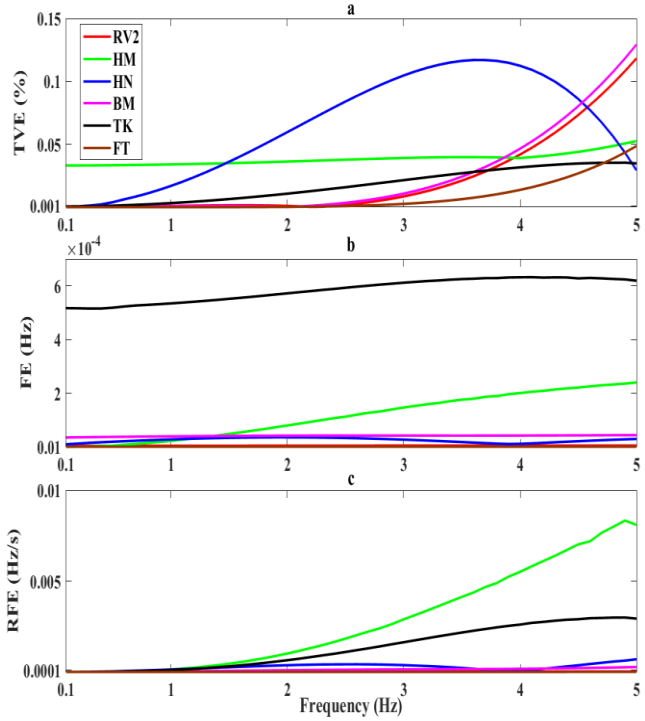

Fig. 8. (a) TVE, (b) FE and (c) RFE under magnitude modulation test

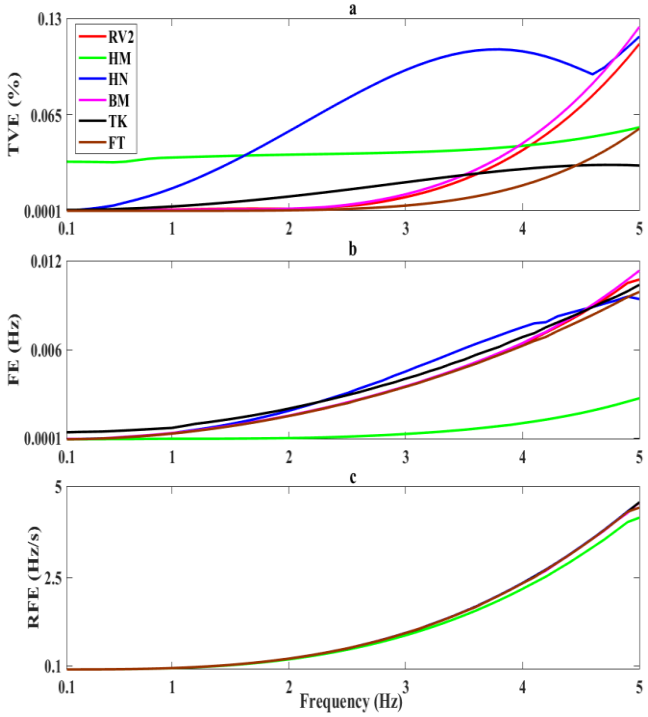

Fig. 9. (a) TVE, (b) FE, and (c) RFE under phase modulation test

2) Phase modulation test

The phase angle of the dynamic state signal is modulated as given in (30) with the parameters k_{pmd} = 0.1, and the modulating frequency w_{md} for the range of 0.1 to 5 Hz with a step of 0.1 Hz.

$$x(t) = x_m \cos\left[\omega_0 t + k_{pmd} \cos(\omega_{md} t - \pi)\right] \quad (30)$$

Figure 9(a) demonstrates that all windows under phase modulation have less TVE than the limit of 3%. In the phase modulation test, the TVEs produced by the Tukey and FT windows have the closest lowest error. Figure 9(b) shows the FE during the phase modulation test. It is observed that all window functions give a FE less than the maximum limit of 0.3 Hz. Further, the measurement error of the ROCOF under the phase modulation test is shown in Fig. 9(c), which demonstrates that the RFE of all windows is below the limit of 14 Hz/s. In the overall phase modulation test, the Tukey, RV2 and FT windows outperform than other window functions.

3) Frequency ramp test

The effectiveness of the phasor estimation is evaluated under the frequency ramping test using (31) as

$$x(t) = x_m \cos\left(\omega_0 t + \pi R_f t^2\right), \quad (31)$$

where R_f is the frequency ramp rate in Hz/s. A dynamic-state signal is generated with a 100% magnitude, nominal frequency of w_0, and ramp rate (R_f) of ± 1 Hz/s. The positive frequency ramp signal begins at 45 Hz and increases until it reaches 55 Hz. Similarly, the negative frequency ramp test is performed from 55 Hz to 45 Hz. Figures 10(a) and 11(a) depict the TVE measured during the positive and negative ramp tests, respectively. The TVE produced by all windows is less than the limit of 1%. The Tukey, RV2 and FT windows give the lower TVE than other windows. Figures 10(b) and 11(b) show the FE under positive and negative frequency ramp tests, respectively.

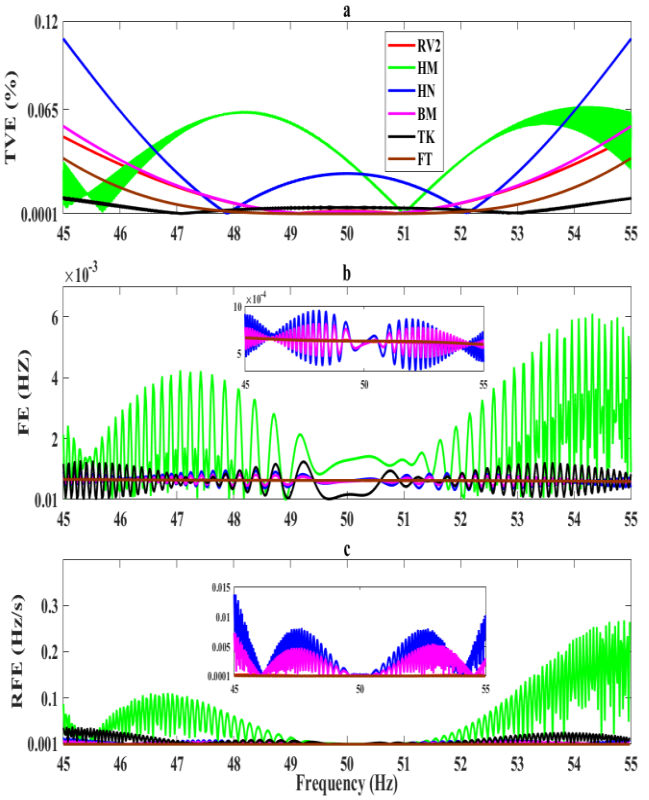

Fig. 10. (a) TVE, (b) FE, and (c) RFE under positive ramp test

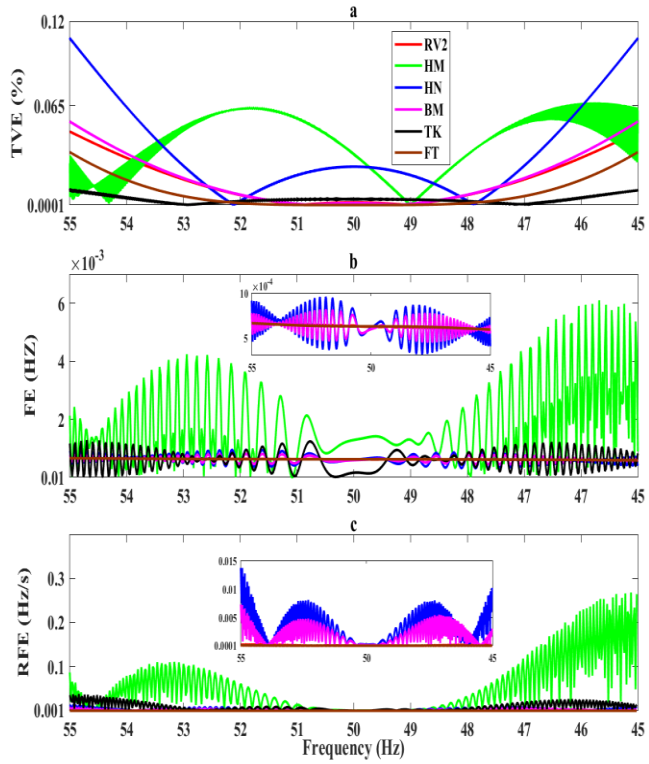

Fig. 11. (a) TVE, (b) FE, and (c) RFE under negative ramp test

The FE of all window functions guarantees that the error does not exceed the limit of 0.01 Hz. The FE of the Tukey, RV2 and FT windows closely tracks, which ismuch lower than the limit of 0.01 Hz. Figures 10(c) and 11(c) show the results of an evaluation of the ROCOF estimator while being subjected to a frequency ramp test. The results show that all other windows successfully fulfil the criteria. Almost all windows give the same level of error which is much lower than the limit of 0.2 Hz/s.

4) Step response test

The step response evaluation measures the delay time, response time, and overshoot of the phasor estimating approach while the step changes occur in magnitude and phase angle [21]. The modeling of the step change of magnitude and phase is performed as

$$x(t) = x_m[1 + S_{ms}\, g(t)] \times \cos\left(w_o t + S_{ps}\, g(t)\right) \quad (32)$$

$$g(t) = \begin{cases} 0, & t < t_1 \\ 1, & t \geq t_1 \end{cases} \quad (33)$$

where, $g(t)$ is the function of a unit step function, S_{ms} is the step size of magnitude, S_{ps} is the step size of the phase angle. The t_1 is the time instant at which the step change occurs. The delay time is the amount of time that must pass until the estimated phasor reaches 50% of the step change from t_1 as shown in Fig. 12(a) and Fig. 13(a). On the other hand, the response time is the amount of time that must pass between the moment that the TVE of the estimated phasor falls below 1% and the instant the TVE rises above 1% after the step changes as shown in Figures 12(b) and 13(b). The overshoot is the difference between the highest value that is reached during the transition and the steady-state value that is reached after the step change.

Step change in magnitude

The step response test with a step change in magnitude is carried out by setting the S_{ms} = 0.1 and S_{ps} = 0 in Eqn. (32). The test is performed with a change in the magnitude from 100% to 110% at 1 s (t_1) as shown in Fig. 12(a). While performing the step change in the magnitude angle test, the frequency is kept at the nominal frequency and the phase angle is zero.

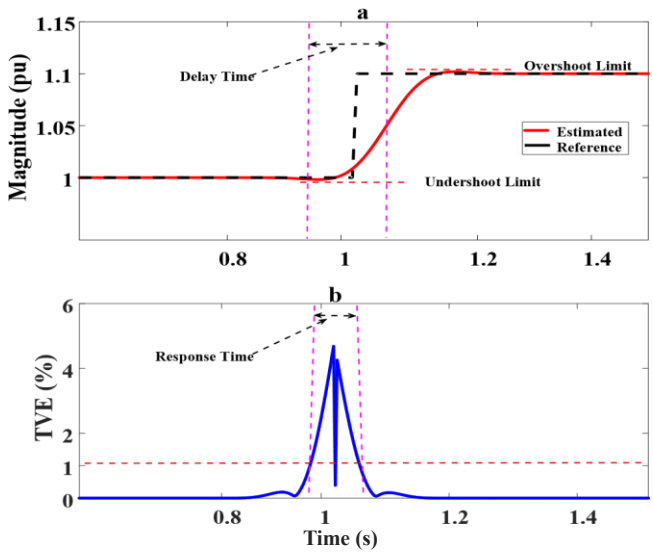

Fig. 12. Step change in magnitude (a), and TVE (b)

Step change in phase angle

The step response test with a step change in phase angle is accomplished by setting the S_{ms} = 0 and S_{ps} = π/18 in Eqn. (32). The test is performed with a change in the phase angle from 0° to 10° at 1 s (t_1) as shown in Fig. 13(a). While performing the step change in the phase angle test, the frequency is kept at the fundamental frequency and the magnitude is 100%.

The performance of the various windows of the FIR filter is evaluated and given in Table 1. The indices reveal that the FT, RV2 and Tukey window functions perform well in overall aspects of the step response.

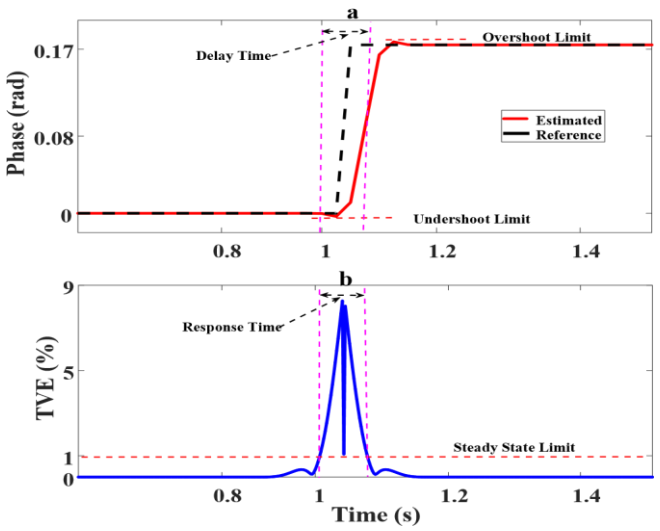

Fig. 13. Step change in phase angle (a), and TVE (b)

4.3 Comprehensive analysis

The maximum values of TVE, FE and RFE of window functions RV2, Hamming, Hanning, Blackman, Tukey, and Flat-top used in the band-pass FIR filter under steady-state and dynamic-state testing are given in Table 1. The results reveal that all window functions used in the band-pass FIR filter for phasor estimation fulfil the requirement criteria. It is noted that the Flat-top window function offers the least error in the maximum number of steady-state tests and the Tukey window function produces the least error in the dynamic-state tests. Whereas, the RV2 window function gives a moderate error which is better than other window functions. it is found that the error produced by the Hamming window is almost close to the maximum error limit in many tests. In addition, the step response test results show that the Flat-Top offers the least response and delay times, whereas in overshoot measurement, RV2 gives the lowest value. It is observed that Flat-top, RV2 and Tukey window functions offer low error competitively in all tests. The performance enhanced M-class phasor estimation using band-pass FIR filter offers the least error than the other approaches reported in the literature [15, 16] at a given low sampling rate of 800 Hz.

Table 1. Maximum values of TVE, FE and RFE under steady and dynamic state tests

TVE(%)							
Test		RV2	HM	HN	BM	TK	FT
FR		8.89×10^{-6}	6.31×10^{-2}	6.16×10^{-4}	2.88×10^{-4}	1.9×10^{-3}	2.41×10^{-6}
MR		4.5×10^{-6}	3.32×10^{-2}	2.37×10^{-5}	3.87×10^{-5}	2.61×10^{-4}	8.31×10^{-7}
HD	2*nd*	3.13×10^{-5}	0.0416	3.36×10^{-4}	1.28×10^{-4}	7.0×10^{-4}	1.65×10^{-5}
	3*rd*	1.28×10^{-5}	0.0391	3.17×10^{-5}	4.88×10^{-5}	6.19×10^{-4}	8.77×10^{-6}
OOB	47.5	8.5×10^{-3}	8.77×10^{-2}	8.3×10^{-4}	1.8×10^{-4}	8.6×10^{-4}	0.013121
	50	8.32×10^{-3}	6.14×10^{-2}	7.31×10^{-3}	1.75×10^{-3}	8.45×10^{-4}	0.013065
	52.5	8.52×10^{-3}	7.53×10^{-2}	8.51×10^{-3}	1.83×10^{-3}	8.41×10^{-3}	0.0130667
MM		0.1183	5.25×10^{-2}	0.1175	0.1293	3.48×10^{-2}	4.86×10^{-2}
PM		0.1127	5.64×10^{-2}	0.1176	0.1242	3.06×10^{-2}	5.55×10^{-2}
Ramp	+ve	0.0480	0.0671	0.109	0.0545	0.0103	0.0346
	-ve	0.0480	0.0671	0.108	0.0545	0.0103	0.0346
FE (Hz)							
FR		5.05×10^{-6}	4.52×10^{-2}	2.93×10^{-4}	1.74×10^{-4}	3.4×10^{-4}	1.44×10^{-6}
HD	2*nd*	6.27×10^{-6}	2.7×10^{-4}	6.76×10^{-5}	8.11×10^{-5}	5.25×10^{-4}	3.08×10^{-6}
	3*rd*	3.65×10^{-6}	1.58×10^{-4}	1.12×10^{-5}	3.36×10^{-5}	4.49×10^{-4}	6.74×10^{-7}
OOB	47.5	2.4×10^{-3}	9.86×10^{-3}	2.31×10^{-3}	6.58×10^{-4}	2.5×10^{-3}	3.65×10^{-3}
	50	2.23×10^{-3}	6.62×10^{-3}	2.21×10^{-3}	4.9×10^{-4}	2.63×10^{-3}	1.86×10^{-3}
	52.5	2.43×10^{-3}	9.1×10^{-3}	2.31×10^{-3}	6.44×10^{-4}	2.32×10^{-3}	3.61×10^{-3}
MM		4.85×10^{-6}	2.39×10^{-4}	2.95×10^{-5}	4.37×10^{-5}	6.19×10^{-4}	9.07×10^{-7}
PM		1.07×10^{-2}	2.83×10^{-3}	9.41×10^{-3}	1.13×10^{-2}	1.04×10^{-2}	9.91×10^{-3}
Ramp	+ve	6.58×10^{-4}	6.1×10^{-3}	9.54×10^{-4}	8.12×10^{-4}	1.3×10^{-3}	6.61×10^{-4}
	-ve	6.56×10^{-4}	6.1×10^{-3}	9.35×10^{-4}	8.05×10^{-4}	1.3×10^{-3}	6.61×10^{-4}
RFE (Hz/s)							
FR		2.42×10^{-4}	0.2593	1.45×10^{-2}	7.83×10^{-3}	1.67×10^{-2}	8.78×10^{-5}
HD	2*nd*	4.13×10^{-9}	7.9×10^{-3}	1.55×10^{-5}	5.96×10^{-6}	7.44×10^{-7}	1.29×10^{-8}
	3*rd*	4.51×10^{-9}	7.9×10^{-3}	1.57×10^{-5}	5.98×10^{-6}	6.37×10^{-7}	1.25×10^{-8}
OOB	47.5	0.2307	0.6835	0.2086	4.9×10^{-3}	0.2255	0.3521
	50	0.2153	0.644	0.1932	4.46×10^{-2}	0.2134	0.1748
	52.5	0.2308	0.6892	0.2111	5.16×10^{-2}	0.223	0.3522
MM		2.27×10^{-5}	8.1×10^{-3}	6.98×10^{-4}	2.69×10^{-4}	2.95×10^{-3}	4.66×10^{-6}
PM		4.5491	4.1401	4.5532	4.5632	4.5624	4.4144
Ramp	+ve	2.69×10^{-4}	0.2681	0.0137	7.34×10^{-3}	0.0378	9.71×10^{-5}
	-ve	2.73×10^{-4}	0.2682	0.0143	7.54×10^{-3}	0.0379	9.16×10^{-5}
Step Change in Magnitude							
Response Time (s)		0.0288	0.041	0.0463	0.03	0.025	0.0224
Delay Time (s)		0.0562	0.0525	0.075	0.0562	0.075	0.0451
Max Over Shoot		0.3636	0.5454	0.5454	0.3636	0.5454	0.4234
Step Change in Angle							
Response Time (s)		0.041	0.04	0.0465	0.041	0.0397	0.021
Delay Time (s)		0.005	0.0062	0.0062	0.005	0.005	0.005
Max Over Shoot		3.2081	4.2979	6.1318	5.2722	5.3291	5.6219

5 Conclusion

The work presents the enhanced M-class phasor estimation using the band-pass FIR filter. The performance enhancement of the band-pass FIR filter for phasor estimation is achieved with the magnitude correction factor. A rigorous performance analysis of the enhanced phasor estimation using the band-pass FIR filter with various window functions RV2, Hamming. Hanning, Blackman, Tukey, and Flat-top is evaluated under standard steady and dynamic tests. The results show that the enhanced phasor estimation with a low sampling rate produces less error than the reported work. The Flat-Top, RV2 and Tukey window functions offer significantly less error than the maximum limit in all tests prescribed in the standards. The work shows that the phasor estimation using band-pass FIR filter offers promising performance over the off-nominal frequency band than other approaches reported in the literature. The performance enhancement is attained with less computation and a low sampling rate. Therefore, it may be recommended for the phasor measurement at distribution network applications.

Acknowledgement

This work is supported by the Science and Engineering Research Board under the Start-up Research Grant Scheme (SRG/2021/001837).

References

[1] R. K. Mai, Z. Y. He, L. Fu, B. Kirby, and Z. Q. Bo, "A dynamic synchrophasor estimation algorithm for online application," *IEEE Transactions on Power Delivery*, vol. 25, no. 2, pp. 570–578, 2010.

[2] D. Belega, D. Macii, and D. Petri, "Fast synchrophasor estimation by means of frequency-domain and time-domain algorithms," *IEEE Transactions on Instrumentation and Measurement*, vol. 63, no. 2, pp. 388–401, 2014.

[3] D. Belega, D. Fontanelli, and D. Petri, "Low-complexity least-squares dynamic synchrophasor estimation based on the discrete Fourier Transform," *IEEE Transactions on Instrumentation and Measurement*, vol. 64, no. 12, pp. 3284–3296, 2015.

[4] A. Zamora, "Digital filter for phasor estimation applied to distance relays," *IET Generation, Transmission Distribution*, vol. 9, pp. 1954– 1963(9), November 2015.

[5] "IEEE/IEC International Standard - Measuring relays and protection equipment - part 118-1: Synchrophasor for power systems measurements," *IEC/IEEE 60255-118-1:2018*, pp. 1–78, 2018.

[6] H. Liu, T. Bi, and Q. Yang, "The evaluation of phasor measurement units and their dynamic behavior analysis," *IEEE Transactions on Instrumentation and Measurement*, vol. 62, no. 6, pp. 1479–1485, 2013.

[7] T. Bi, H. Liu, Q. Feng, C. Qian, and Y. Liu, "Dynamic phasor model based synchrophasor estimation algorithm for M-class PMU," *IEEE Transactions on Power Delivery*, vol. 30, no. 3, pp. 1162–1171, 2015.

[8] D. Belega and D. Petri, "Accuracy analysis of the multicycle synchrophasor estimator provided by the interpolated DFT algorithm," *IEEE Transactions on Instrumentation and Measurement*, vol. 62, no. 5, pp. 942–953, 2013.

[9] P. Romano and M. Paolone, "Enhanced interpolated-DFT for synchrophasor estimation in FPGAs: Theory, implementation, and validation of a PMU prototype," *IEEE Transactions on Instrumentation and Measurement*, vol. 63, no. 12, pp. 2824–2836, 2014.

[10] D. Belega, D. Fontanelli, and D. Petri, "Dynamic phasor and frequency measurements by an improved Taylor weighted least squares algorithm," *IEEE Transactions on Instrumentation and Measurement*, vol. 64, no. 8, pp. 2165–2178, 2015.

[11] S. Xu, H. Liu, T. Bi, and K. Martin, "An improved Taylor weighted least squares method for estimating synchrophasor," *International Journal of Electrical Power Energy Systems*, vol. 120, p. 105987, 2020.

[12] S. Affijulla and P. Tripathy, "Development of phasor estimation algorithm for P-class PMU suitable in protection applications," *IEEE Transactions on Smart Grid*, vol. 9, no. 2, pp. 1250–1260, 2018.

[13] S. Affijulla and P. Tripathy, "Estimation of phasor under dynamic conditions using convolution," in *2015 IEEE Power Energy Society General Meeting*, pp. 1–5, 2015.

[14] S. Hampannavar, C. Teja, M. Swapna, and U. Kumar R.Y., "Performance improvement of m-class phasor measurement unit (PMU) using hamming and blackman windows," in *2020 IEEE International Conference on Power Electronics, Smart Grid and Renewable Energy (PESGRE2020)*, pp. 1–5, 2020.

[15] J. R. Razo-Hernandez, A. Mejia-Barron, D. Granados-Lieberman, M. Valtierra-Rodriguez, and J. F. Gomez-Aguilar, "A new phasor estimator for PMU applications: P-class and M-class," *Journal of Modern Power Systems and Clean Energy*, vol. 8, no. 1, pp. 55–66, 2020.

[16] K. Duda and T. P. Zielinski, "Fir filters compliant with the IEEE standard′ for M-class PMU," *Metrology and Measurement Systems*, vol. vol. 23, no. No 4, pp. 623–636, 2016.

[17] C. Thilakarathne, L. Meegahapola, and N. Fernando, "Improved synchrophasor models for power system dynamic stability evaluation based on IEEE C37.118.1 reference architecture," *IEEE Transactions on Instrumentation and Measurement*, vol. 66, no. 11, pp. 2937–2947, 2017.

[18] A. J. Roscoe, B. Dickerson, and K. E. Martin, "Filter design masks for C37.118.1a-compliant frequency-tracking and fixed-filter M-class phasor measurement units," *IEEE Transactions on Instrumentation and Measurement*, vol. 64, no. 8, pp. 2096–2107, 2015.

[19] D. Agrez and T. Luˇ sin, "Non-parametric estimation of the amplitudeˇ ratio of sinusoidal signals with common frequency," *Measurement*, vol. 55, pp. 176–185, 2014.

[20] F. Harris, "On the use of windows for harmonic analysis with the discrete Fourier transform," *Proceedings of the IEEE*, vol. 66, no. 1, pp. 51–83, 1978.

[21] J. Khodaparast, O. B. Fosso, and M. Molinas, "Phasor estimation by EMD-assisted Prony," *IEEE Transactions on Power Delivery*, vol. 37, no. 6, pp. 4736–4748, 2022.

Received 1 January 2024